2011

Hemorrhage correlation with total energy and surface power near opossum skull exposed to pulsed ultrasound

Viksit Kumar
Iowa State University

Hemorrhage correlation with total energy and surface power near opossum skull

exposed to pulsed ultrasound

by

Viksit Kumar

A thesis submitted to the graduate faculty

in partial fulfillment of the requirements for the degree of

MASTER OF SCIENCE

Major: Mechanical Engineering

Program of Study Committee:

Timothy Bigelow, Major Professor

Donald Sakaguchi

Pranav Shrotriya

Iowa State University

Ames, Iowa

2011

TABLE OF CONTENTS

LIST OF FIGURES

LIST OF TABLES

ABSTRACT

High intensity focused ultrasound (HIFU) has been used noninvasively for therapeutic applications. Previous studies have shown that HIFU when targeted on fetal rat and mice bones resulted in hemorrhage. Hemorrhage occurrence and area were found to correlate with total equivalent energy (i.e. product of energy density, number of pulses and volume of the focal region) and surface power (i.e. product of pulse average intensity, number of pulses and beam area). Continuation of the trend was observed in Opossum pups. Opossum pups (7- 8 post natal days) were exposed to 1.1 MHZ f/1 spherically focused transducer (6.3 cm focal length). Three groups of n=8 and a control group of n=8 were exposed to rarefactional pressure of 6, 4.5, 3.6 MPa with ITA values of 10.78, 5.39, 6.74 W/cm^2. PRF was varied by 500, 500, 1000 Hz with an exposure duration of 2 to 4 minutes. Dependence of hemorrhage on total energy and surface power suggests mechanical failure to be a possible mechanism.

CHAPTER 1. INTRODUCTION

In the United States alone, over 150,000 infants are born every year with serious birth defects (~3% of the babies born) as reported by the National center for health statistics (NCHS). This estimate does not include 25% of the stillborn babies which have birth defect according to the Wisconsin still birth program. Serious defects are the leading cause of death in the first year of life and are responsible for 20% of all infant deaths in 2000 according to NCHS. In addition to the emotional cost associated with the loss of an infant or fetus, serious birth defects have a large economic cost exceeding an estimated eight billion dollars a year according to the March of Dimes foundation. The impact of some birth defects can be reduced by surgery on the fetus before birth. Recently some defects that have benefited from fetal surgery are provided in Appendix. However, surgical intervention on the developing fetus is hindered in many applications by the accompanying risks such as dramatic increase in the occurrence of preterm labor, chorioamniotic membrane separation, preterm premature rupture of the membranes and altered fetal hemostasis [1]. Due to the complications and risks involved in the fetal surgery, it is typically reserved for the most extreme or life threatening defects. Many of the risks associated with fetal surgery can be reduced by adapting the surgery to be minimally invasive [1]. Therefore, enabling technology needs to be developed that is minimally invasive and applicable to fetal therapeutic interventions.

Ultrasound is a cyclic pressure wave with frequency greater than 20,000Hz. For many years ultrasound has been used for diagnostic purposes. Recently ultrasound has been successfully used to non-invasively target a tissue region of interest in therapeutic

applications. Ultrasound therapy often involves thermal ablation where tissue necrosis is induced by elevated temperatures during ultrasound exposures [2-8]. However ultrasound has also been used for removing tissue in a controlled manner [9-11], gene transfection [12-20], localized drug delivery [21, 22] and the acceleration of thrombolysis [23]. However, the use of ultrasound in therapeutic applications for the fetus remains largely neglected despite its non-invasive properties. For example, congenital cystic adenomatoid malformation, Sacrococcygeal Teratoma, twin reversed arterial perfusion syndrome, and twin-twin transfusion syndrome are selected problems that could potentially benefit from noninvasive ultrasound ablation. For some rare patients, congenital cystic adenomatoid malformation [24] and Sacrococcygeal Teratoma [25] are treated by surgical resection increasing the risk of pre-term delivery thus increasing the potential for further complications after birth. It may be possible to replace the surgical resection with ultrasound ablation. Also, twin-twin transfusion syndrome has been successfully treated by using a laser inserted into womb to ablate tissue separating the two fetal circulation systems (minimally invasive) often under ultrasound guidance [26]. It may be possible to make the treatment completely noninvasive using ultrasound ablation. Twin reversed arterial perfusion syndrome is already being considered for treatment by ultrasound thermal ablation by some investigators [27]. In addition to thermal ablation applications, ultrasound assisted gene therapy [12-20] might be very useful for treating genetic diseases before birth when applied to the fetus.

Before ultrasound therapy can be developed for a fetus, the related bioeffects associated with the interaction of ultrasound with the tissue should be understood, predicted and precisely controlled so that the safety and effectiveness of the therapy can be maximized.

Identifying the mechanism responsible for bioeffects is the best way to minimize the risk during any given exposure. The mechanism may vary depending on the ultrasound parameters and the targeted tissue. Soft tissue may have different bioeffects compared to tissue near bone. Possible mechanism includes thermal heating, radiation force, streaming, inertial cavitation or a combination of these mechanism acting together [28]. Identifying the mechanism can help in predicting and controlling the bioeffect related with the mechanism. The parameters associated with the mechanism can also be controlled to remove the occurrence of bioeffect or made to occur in a controlled environment. For example, if a thermal legion is generated upon exposure to ultrasound, the formation of the lesion can be predicted by estimating the *in vivo* time-average intensity and solving the bioheat transfer equation while estimating or approximating the values for tissue perfusion, thermal conductivity and specific heat [29]. To lower or remove the bioeffect the parameters in the bioheat transfer equation can be tuned to desired value. Similarly if a harmful bioeffect is due to inertial cavitation, the occurrence of the bioeffect can be predicted from the *in vivo* peak rarefactional pressure and frequency. Controlling the pressure and frequency can help to avoid inertial cavitation. However, even if the mechanism responsible for damage cannot be determined conclusively, an increased understanding of how the damage develops for different exposure conditions would help improve the safety and effectiveness of therapy planning.

In addition to the therapeutic benefits of the study, increasing the understanding of ultrasound induced bioeffects is critical in maintaining the safety of diagnostic ultrasound [30]. Identifying the mechanism for bioeffect will be important if the maximum allowed

ultrasound exposures in obstetric ultrasound are ever redefined in terms of actual risk to the fetus. The current allowed outputs are based on the largest output intensities available in 1976 and are not based on safety considerations for fetus [30]. The current safety standard puts a limit on the time-average intensity to 720 mw/cm^2, it does not consider the possibility of an increased risk of mechanical bioeffects due to the presence of bone at the focus [31]. Thermal index for bone (TIB) is the only safety parameter for bone at the focus which estimates the risk of heating due to bone.

One fatal bioeffect that is not well understood is hemorrhage near developing fetal bone from exposure to pulsed ultrasound at diagnostic frequencies. The current study focuses on determining the mechanism and controlling parameters behind the ultrasound induced hemorrhage. Hemorrhage near the developing fetal skull is an ultrasound related bioeffect that has been observed and should be avoided when ablating fetal tissue or performing gene therapy. Hemorrhage occurs when there is a loss of blood from the circulatory system and can lead to serious medical conditions or even death.

When determining if a particular mechanism is responsible for an observed bioeffect, it is important to quantify the relative importance of other mechanisms. Isolating the influence of each mechanism is challenging due to ultrasound exposure parameters impacting more than one mechanism. For example, increasing the time average intensity of the ultrasound increases both the resulting temperature and the radiation force. The major mechanisms and their controlling parameters are discussed in the next chapter.

CHAPTER 2. MECHANISMS

The major bioeffects that will be covered in this study are thermal heating, inertial cavitation, radiation pressure and mechanical effect. Details about the mechanism and their influencing parameters will play a vital role in concluding which mechanism is responsible for causing hemorrhage near fetal skull.

2.1 Thermal heating

2.1.1 Introduction

The biological effect of thermal heating has been studied for many years by many different investigators [32-39]. Potential bioeffects due to heating in fetus need to be examined separately due to the sensitive nature of the tissue and potential impact on the growth of developing fetus [40]. Both diagnostic and therapeutic ultrasound can raise the temperature in fetal tissues to the extent that it can harm the targeted tissue. The extent of the damage done depends on the scanning mode, exposure parameters and the tissue being targeted. Non-human studies have shown that temperature increase of greater than 4 degree Celsius for an exposure period of greater than 5 minutes can cause developmental abnormalities. Although the temperature rise from diagnostic ultrasound is not expected to be large enough to cause any serious bioeffects, whereas the settings used in therapeutic ultrasound can easily cause thermal related bioeffects.

As ultrasound wave travels in an attenuating medium such as soft tissues and bone the amplitude and the energy of the wave decreases with the distance travelled. This loss of energy is caused by absorption and scattering of the ultrasound wave travelling in the medium. Absorption loss occurs due to the wave energy being converted into heat as it passes through the attenuating medium and scattering loss is the wave energy that has been reflected by the medium resulting in the images seen on the screen. Since the medium is attenuating in nature and it absorbs the energy transmitting through it, this results in a temperature increase if the rate at which heat is being generated is greater than the rate at which it is dissipated. This local rise in temperature can cause serious thermal damage.

Bones have a higher attenuation/absorption coefficient as compared to soft tissues resulting in more heat generation [34, 41]. The impact of bone on heating has been well established with extensive experimental results obtained from the developing fetal guinea-pig and sheep skull [42-48]. The amount of heat generated in the medium is associated with the thermal index (TI) of the medium. Thermal index is defined as the ratio of total acoustic power to the power required to raise the temperature by $1^{o}C$ in an assumed model. Due to the varying exposure conditions and tissue types a TI increase of 1 does not necessarily mean an increase in temperature by $1^{o}C$. Efforts are being made to define TI for all varying conditions but almost every scanning condition departs in some respects from the assumed conditions in the numerical model. The increased heating with bone is the reason that the thermal index for diagnostic ultrasound is different when there is bone at the focus [31]. Thermal index for bone (TIB) is used instead of TI for soft tissues when bone is at the focus. A good example is the ossifying bone in fetus where TIB is used instead of TI.

Bone attenuation typically increases with increasing bone density, at least for frequencies less than 1.5 to 2 MHz [49-52]. For this reason, ultrasound induced heating is greater as the gestational age of the fetus increases [34]. Fortunately, the bioeffects associated with heating that have been studied to date are typically more significant early on in the gestational period during organogenesis before bone has developed [53-55]. The bioeffects associated with heating also depends on the total time that the temperature has been elevated above normal body temperature and not just on the magnitude of the temperature increase [56]. Hence, exposure duration normally plays a role in temperature related bioeffects.

Bone can also increase ultrasound induced heating by generation and propagation of shear waves [57, 58]. Bone, due to its structure, can support shear waves while soft tissues normally does not at ultrasound frequencies. The absorption of shear waves in bone is much greater than the absorption of longitudinal waves resulting in a greater rate of heating and a larger temperature increase. The coupling of energy into shear waves in the bone depends on the angle at which the ultrasound waves impinge on the soft-tissue bone interface [57, 58].

In addition to increased heating due to the attenuation of bone, the ultrasound induced temperature rise also depends on the amount of blood perfusion near the bone [48, 59]. Although the influence of perfusion is less for narrower beams [60] as well as for fetuses at younger gestational ages before the blood vessels have had time to develop [46]. While the cooling effects of blood perfusion on the skull are more significant for broader beams, the resulting temperature increase is typically larger for the same average ultrasound beam intensity due to the increased size of the heat source resulting in less thermal diffusion [32].

2.1.2 Bioheat transfer equation

Due to the large number of biological effects related with temperature change in tissue, considerable interest has been shown in the propagation of temperature variation in the human body. An approximate temperature increase in the fetal skull as a function of time, assuming all of the heating is due to sound absorption in an infinitesimally thin layer, is approximately given by [32].

$$T(t) = \int_0^\infty \frac{\phi I(r)}{4K} \{e^{-r/L}[2 - \text{erfc}(\sqrt{t/\tau} - r/\sqrt{4\kappa t})] + e^{r/l}\text{erfc}(\sqrt{t/\tau} + r/\sqrt{4\kappa t})\}dr \qquad (2.1)$$

where κ is the thermal diffusivity of the medium; τ is the time constant for perfusion; L is the perfusion length (L=$\sqrt{\kappa t}$); K is the thermal conductivity coefficient; Φ is a dimensionless quantity that gives the fraction of the incident energy that is absorbed; r is the radial distance perpendicular to the beam axis (along the thin bone layer where the sound is absorbed); I(r) is the incident temporal-average intensity at r assuming circular symmetry about the beam axis. For calculation purposes, K=0.6 W/m-°C; κ=1.4 $\times$ 10^{-7} m^2/s; τ=100s and Φ=0.6 [32]. I(r) used in these calculation is given by

$$I(r) = I_{TA} \left[\frac{2J_1(\frac{\pi r}{\lambda(f\#)})}{\frac{\pi r}{\lambda(f\#)}}\right]^2 \qquad (2.2)$$

where the location of I_{TA} is at the focus; λ is the wavelength of the sound; f# is the f number for the source.

2.1.3 Parameters related to thermal heating

From the bioheat transfer equation (2.1), we can conclude that the temperature rise as a function of time is mainly dependent on the time-average intensity and the exposure duration since all other parameters are constant. The local temperature should increase both with increasing time-average intensity and exposure duration.

2.2 Inertial cavitation

2.2.1 Introduction

Inertial cavitation is one of the primary non thermal bioeffects which is caused by the interaction of ultrasound wave with gas bubbles. It is often simply referred as cavitation. Gas bubbles are small pockets of gas spread throughout the body. Lungs and intestines naturally harbor gas bodies (i.e., microbubble) whereas they are absent in most of the biological tissue [61]. The dramatic expansion and sudden collapse of these gas bodies in a fluid medium upon exposure to ultrasound is called cavitation. The cavitation of the microbubble is driven by a negative rarefactional pressure that causes the bubble to expand followed by a positive compressional pressure that forces the bubble to collapse. For every microbubble, an ultrasound pressure threshold for inertial cavitation exists below which inertial cavitation will not occur. For inertial cavitation, the collapse typically destroys or fragments the bubble generating transient pressure inside the bubble from 1,000 to 70,000 atm and transient temperatures from 1,000 to 20,000 K [62]. These high pressure and temperatures can produce chemical radicals that are highly reactive and subsequently short lived. The bubble collapse

also results in fluid streaming in the vicinity of the bubble [63]. The high transient pressure and temperature can be used to destroy cells and can be a serious biohazard. A passive cavitation detector is used to detect cavitation in experimental studies.

The violence of the collapse during cavitation is governed by the inertia of the fluid during the collapse. Therefore, the largest expansion of the microbubble and associated rarefactional pressure are important when assessing the likelihood of inertial cavitation. As a result, the cavitation threshold is often expressed in terms of the peak rarefactional pressure of the ultrasound pulse. The cavitation threshold is known to increase as the frequency of the ultrasound wave increases making it more difficult to produce inertial cavitation at higher frequencies [64, 65]. Also, for any given frequency, bubbles of a specific size undergo the largest change in bubble size during cavitation resulting in the most violent collapses. These bubbles are referred to as resonant sized bubbles. The resonance frequency for a particular bubble also depends weakly on the pressure amplitude used to excite the bubble [66]. Other investigators have shown that inertial cavitation and the associated tissue damage increases with increasing pulse duration [67-71], increasing pulse repetition frequency [68, 72], and increasing bubble concentration [73] since tissue damage normally results from the excitation of a bubble cloud rather than a single bubble. Studying the behavior of bubble clouds is complicated by the coupled oscillations of adjacent bubbles [74, 75].

Inertial cavitation near bone or tissue boundaries has an increased potential for tissue damage due to the formation of microjets [76, 77] and emission of shock waves. Microjets form due to the asymmetric collapse of the bubbles near boundaries and can be used to erode metals

[78-80]. Fortunately, the microbubbles need to be fairly close to the boundary (~ maximum bubble radius during the bubble expansion) before a significant microjet can form.

2.2.2 Parameters related to inertial cavitation

Peak rarefactional pressures, pulse repetition frequency, frequency of the ultrasound wave and bubble concentration are the major factors influencing inertial cavitation. The likelihood of cavitation increases with increasing rarefactional pressure, pulse repetition frequency, bubble concentration and decreasing frequency. The presence of a gas bubble is must for cavitation and a threshold for pressure exists for cavitation.

2.3 Radiation force

2.3.1 Introduction

When ultrasound wave propagates in an attenuating medium, energy is lost due to absorption from the ultrasound wave. This loss in energy results in a formation of energy gradient in the direction of propagation and is associated with the generation of acoustic streaming due to transfer of momentum from ultrasound wave to the fluid. The force exerted by this phenomenon is called radiation force. In the absence of a boundary, radiation force refers to the volume force (in N/m^2) resulting from the absorption of the wave during propagation [81, 82]. For plane wave propagation, this force is given as

$$F = \frac{2\alpha I}{c} \tag{2.3}$$

where α is the absorption coefficient; c is the sound speed; and I is intensity of the acoustic wave temporally averaged over the wave period [81, 82]. Hence, the force exerted on the tissue by the ultrasound wave increases as the tissue absorption or wave intensity increases. Also, if the sound is pulsed or modulated, the radiation force will also be pulsed/modulated allowing for remote palpation [83, 84] and the generation of low frequency shear waves in tissue [85-87]. Therefore, the pulse repetition frequency for pulsed ultrasound could also contribute to bioeffects related to radiation force.

Similar to the loss of momentum due to absorption, momentum can also be transferred out of the wave by impinging on a boundary. In this case, the radiation force acting on the boundary is related to both absorption and the scattering of the waves by the boundary. The simplest boundary for radiation force calculations is a perfectly reflecting or a perfectly absorbing planar boundary where the force is directly proportional to the total power in the ultrasound beam [88, 89]. Therefore, measuring the radiation force for these cases has been extensively used to determine the transmit power for ultrasound therapy sources [90-92]. Other investigators have also calculated the force exerted on a boundary for ultrasound impinging on solid spheres [93], elastic and viscoelastic spherical shells [94], solid cylinders [95-97], and cylindrical shells [98, 99]. In general, the radiation force for these more complicated geometries is related to the properties of the scattered wave and increases as the intensity, I, of the acoustic wave increases. The radiation force exerted by a plane continuous wave on an isotropic elastic sphere immersed in a non viscous medium is given by

$$F = \pi a^2 E Y_p, \tag{2.4}$$

where E is the mean energy density of the incident plane wave; a is the radius of the spherical target and Y_p is the dimensionless factor known as the radiation force function, which accounts for diffraction by the sphere and is the radiation force per unit cross section and unit energy density [95]. For elastic spheres Y_p is a function of ka, ρ^*/ρ, c_1/c, and c_2/c. Where k, ρ and c are the wavenumber, the density, the sound velocity in the surrounding medium; ρ^*, c_1, c_2 are the density and the velocities of longitudinal shear waves of the target material respectively.

2.3.2 Parameters related to radiation force

Temporal average intensity, attenuation coefficient of the medium, and speed of sound are the controlling factors for radiation force. The force increases with intensity and attenuation but decreases with speed of the sound. Radiation force also depends on the geometry of the boundary.

2.4 Mechanical fatigue

2.4.1 Introduction

Fatigue is the progressive and localized damage which occurs when a material is subjected to cyclic loading, leading to formation and growth of microscopic cracks which finally result in fracture of the material much below its ultimate tensile strength. The number of stress cycles a specimen sustains before its failure is described as the fatigue life of the material. The material performance is characterized by an S-N curve which is a graph of the magnitude of a cyclic stress (S) against the logarithmic scale of cycles to failure (N). The rate

of the growth of crack (da) with the number of cycles (dN) is directly proportional to the stress intensity factor as given by Paris' law [100].

$$\frac{da}{dN} \propto \Delta K^m \tag{2.4}$$

Ultrasound wave also causes a cyclic loading on the boundary due to the radiation force acting on the boundary. The presence of positive compressional pressure and negative rarefactional pressure simulates the cyclic nature of ultrasound wave. The number of pulses hitting the boundary is equivalent to the number of stress cycles in a fatigue specimen.

2.4.2 Parameters related to mechanical fatigue

Radiation forces, number of cycles are the ultrasound parameters which affect mechanical fatigue. As these parameters increase, the likelihood of fatigue damage should increase. A threshold limit exists for the pressure below which fatigue will not occur.

CHAPTER 3. THEORETICAL STUDY

Mouse fetal skulls exposed to lithopter [101] and single element pulsed ultrasound [102] have shown hemorrhage near developing bone. Hemorrhage was also observed when rat skulls were exposed to pulsed ultrasound [103]. The data published in these studies have been studied in more details and was the basis of the preliminary study conducted to find the correlation between different exposure parameters to the damage done by hemorrhage. A brief summary of the two studies with the exposure parameters is given below.

3.1 Summary of previous work done

Hemorrhage was observed in mouse fetus when exposed to piezoelectric lithotripter pulse. The hemorrhage was more pronounced in tissues near developing bones [101]. In a following study C3H mice were exposed to single element pulsed ultrasound at diagnostic frequencies to see if hemorrhages occurred in late gestational fetal mice. On the 18th day of gestation the pregnant females were shaved and exposed to different ultrasound exposures. Seven groups along with two control group with 42-90 animals were exposed to varying frequencies, intensities and different transducers. Similar hemorrhages were observed and the authors suggested that relative motion between partially ossified bones and the surrounding tissues may cause damage to fetal blood vessels resulting in hemorrhage.

To investigate if the damage done by hemorrhage in fetal rat skulls could be correlated with temporal-average intensity, Bigelow et al studied the effect of pulsed ultrasound at diagnostic frequencies in Sprague-Dawley rats at a gestational age of 18-19 days. The pregnant rats were exposed to anesthesia and their abdomens were shaved, then incisions were made to remove the tissue layer revealing the uterus. Four groups along with one control group were exposed to varying intensities and pulse repetition frequencies. The authors concluded that hemorrhage occurrence increased slightly with increasing time average intensity as well as peak rarefactional pressure and pulse repetition frequency. But no correlation was found between exposure parameters and the area of hemorrhage. The author hinted towards a thermal or radiation force mechanism. Table 1 shows an overview of

Parameters	Dalecki	Bigelow
Frequency(MHz)	1.2; 2.4; 3.6	0.92
Intensity(W/cm^2)	0.165 - 1.475	1.9 - 9.4
Pulse Duration(µSec)	10	9.6
Exposure Duration(Sec)	180	60
F#(Focal length/Diameter)	1.57; 2.2; 2.64	1
PRF(Hz)	100	100; 250; 500

parameters used by the two authors in their studies.

Table 1. Overview of parameters used in [102] and [103]

3.2 Exposure parameters

Data was taken from both the previous works and was compared with all the dependencies which might be responsible for different mechanisms. Spatial peak temporal average intensity (I_{SPTA}), rarefactional pressure (p_r), rarefactional pressure divided by

frequency, product of rarefactional pressure divided by frequency and pulse repletion frequency (PRF), energy density (ED), number of pulses (N), product of energy density and number of pulses, total energy (product of energy density, number of pulses, volume of focal region), product of pulse average intensity (I_{PA}), beam area and number of pulses are the dependencies which were compared with hemorrhage area and occurrence. A linear fit was done to find out the regression value (r^2) for each dependency. An r^2 value close to 1 would imply a perfect correlation with hemorrhage occurrence and area, whereas an r^2 value close to zero implies no correlation.

3.3 Results

Figure 1. Correlation of hemorrhage occurrence with different exposure parameters including (a) spatial peak temporal average intensity, (b) rarefactional pressure, (c) rarefactional pressure per frequency, (d) product of rarefactional pressure per frequency and pulse repletion frequency

Figure 1 (a) compares I_{SPTA} to hemorrhage occurrence. I_{SPTA} has been plotted because thermal heating and radiation force are more pronounced at higher values of I_{SPTA}. An r^2 value of 0.0425 was found which shows a poor correlation between I_{SPTA} and hemorrhage occurrence. This indicates that thermal heating and radiation force are not the probable mechanisms behind hemorrhage. Figure 1(b, c, d) compares p_r, PRF and frequency of the wave because cavitation damage has been shown to be more significant at higher p_r and PRFs [67, 70, 104]. But cavitation threshold is known to increase with increasing frequency thereby making it more difficult to produce inertial cavitation at higher frequencies [64, 65]. Low r^2 values of 0.0015, 0.0303, and 0.0227 respectively suggest that there is no correlation between cavitation and hemorrhage occurrence. The solid line in the figure denotes the best fitting line.
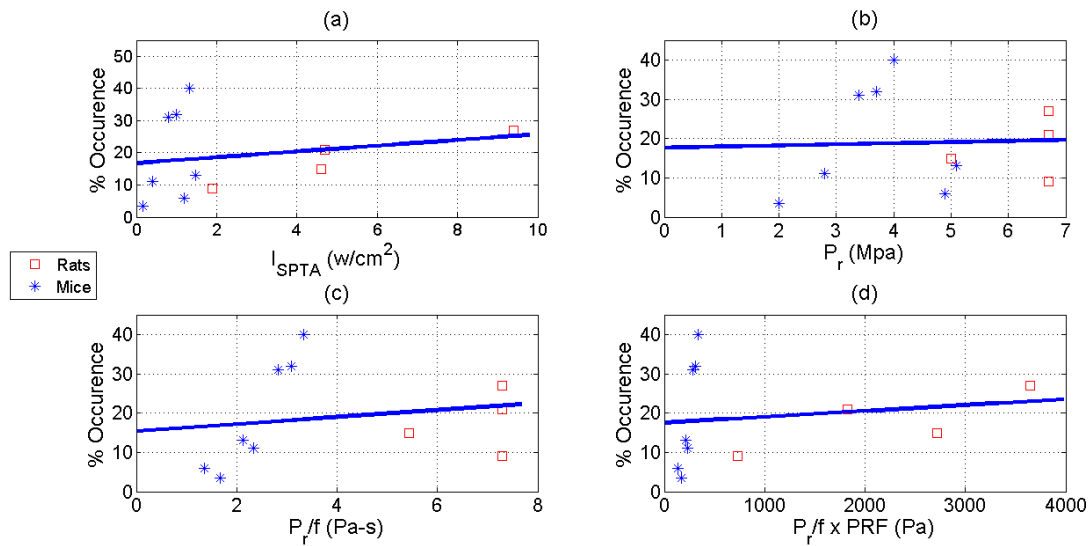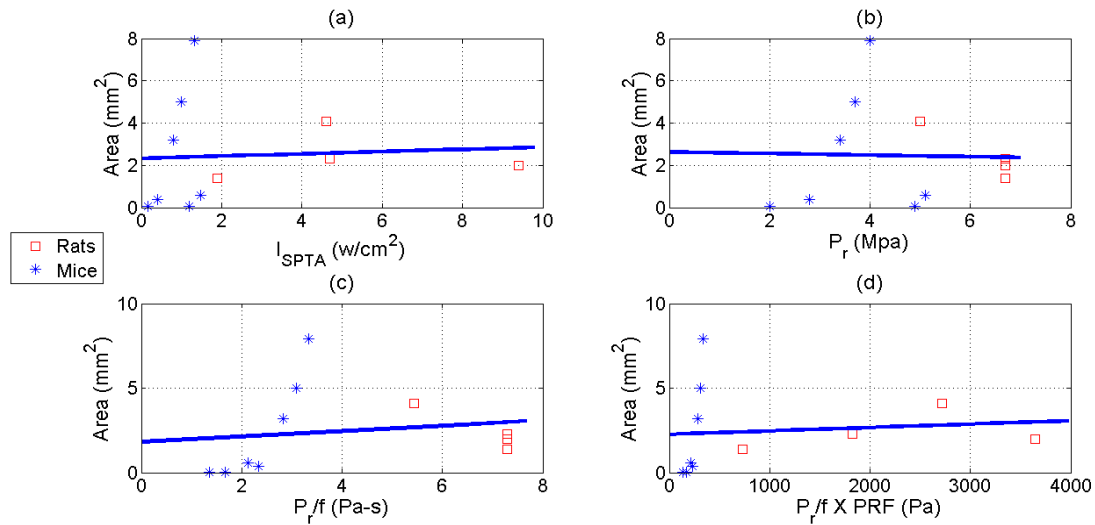

Figure 2. Correlation of hemorrhage area with different exposure parameters including (a) spatial peak temporal average intensity, (b) rarefactional pressure, (c) rarefactional pressure per frequency, (d) product of rarefactional pressure per frequency and pulse repletion frequency

Figure 3. Correlation of hemorrhage occurrence with different exposure parameters including (a) energy density, (b) number of pulses, (c) product of energy density and number of pulses, (d) total energy

Figure 2(a, b, c, d) compare the same dependencies with hemorrhage area. Similar to hemorrhage occurrence, these dependencies show poor correlation with hemorrhage area showing r^2 values of 0.0036, 0.0006, 0.0238 and 0.0100 respectively. Figure 3(a), 4(a) compares energy density with hemorrhage occurrence and area. Energy density term reflects the force exerted on the skull over a pulse by the ultrasound wave. Low r^2 values of 0.0501 and 0.0142 are observed. Radiation force and mechanical mechanism are directly related with energy density. Figure 3(b), 4(b) compare the number of pulses with hemorrhage occurrence and area. The number of pulses is a measure of repetitive damage done by ultrasound wave. Poor correlation is observed with r^2 values of 0.0420 and 0.0289. Figure 3(c), 4(d) tries to combine the terms associated with mechanical and radiation force (energy density and number of pulses) together to find a correlation with hemorrhage area and

occurrence, r^2 values of 0.1379 and 0.0332 are found respectively. A difference in order of magnitude is observed in r^2 values for hemorrhage occurrence when compared to all previous values. This indicates that the product of energy density and number of pulses is

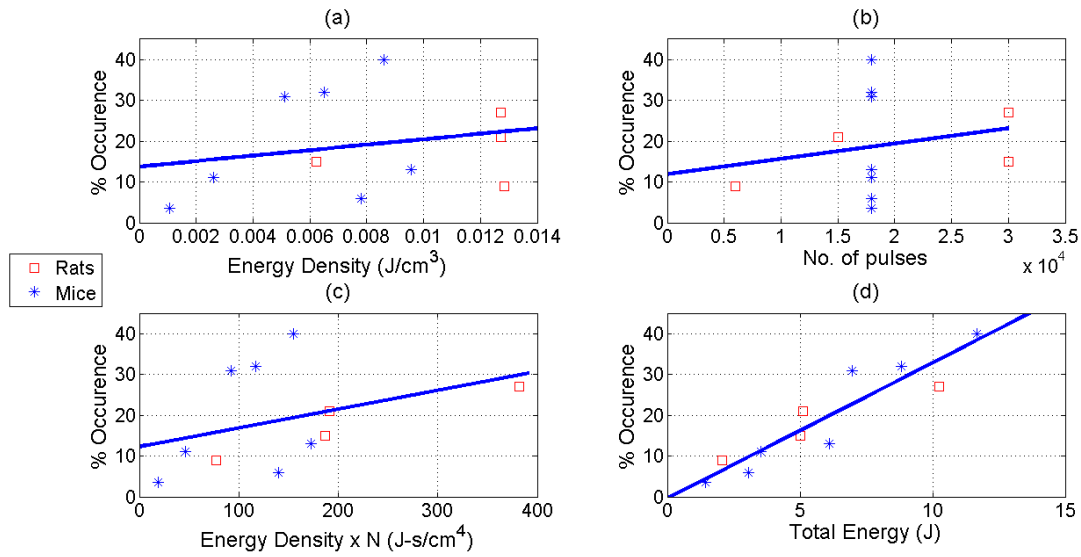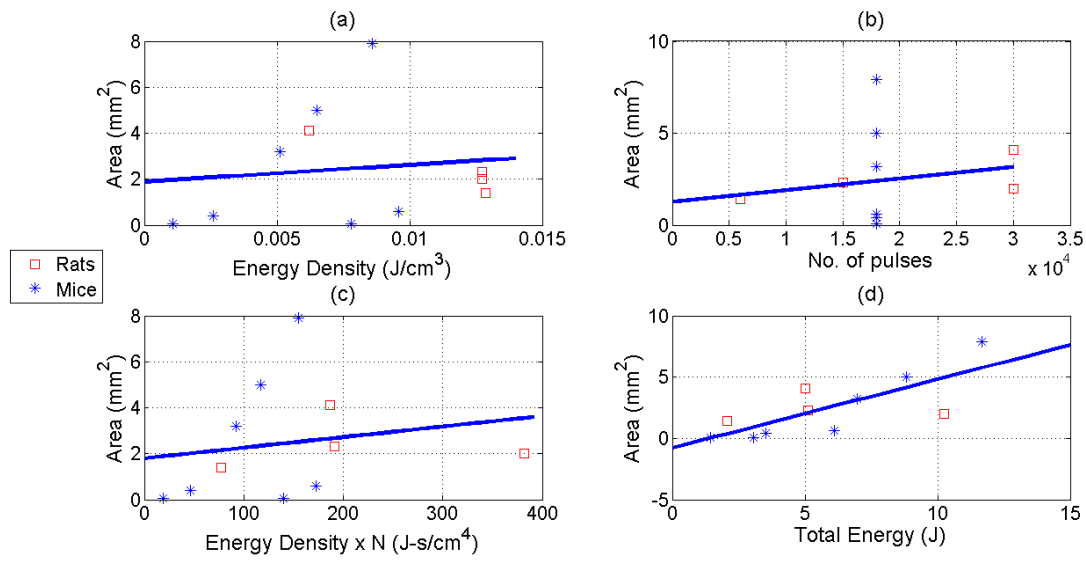**Figure 4.** Correlation of hemorrhage area with different exposure parameters including (a) energy density, (b) number of pulses, (c) product of energy density and number of pulses, (d) total energy

somewhat correlated to the hemorrhage occurrence. To further explore this relation the product of ED and N was multiplied with the volume of the focal region and is called total energy. A very good correlation was found between total energy, and hemorrhage occurrence as well as area with high r^2 values of 0.8519 and 0.5833. The dependence of the hemorrhage on total energy was in accordance with the general observation that if more energy is provided there is a greater chance of doing damage.

To see the effect on surface rather than the volume an additional graph was plotted. Figure 3.5(a, b) tries to correlate the product of I_{PA}, beam area and number of pulses. This

term tries to focus on the surface power associated with the ultrasound exposure. The r^2 values of 0.4579and 0.2480 suggest that the hemorrhage might be a surface phenomenon but does not have as strong correlation as the total energy term. This dependence on volume term is really important and can play a critical role in determining the mechanism behind the hemorrhage.
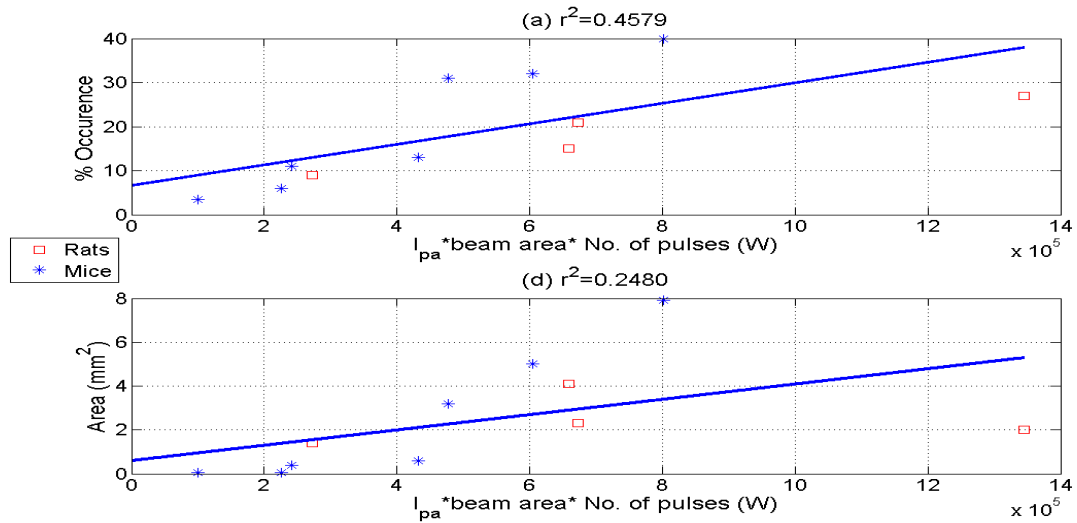
Figure 5. Correlation of product of pulse average intensity, beam area and number of pulses with (a) hemorrhage occurrence, (b) hemorrhage area

CHAPTER 4. EXPERIMENTAL PROCEDURE

Analysis from previous studies has shown that total energy carried by the ultrasound wave correlates with the hemorrhage occurrence and area. The results taken from two different labs and two different animal models showed such strong correlation with total energy term that it became imperative to study if the same trend continued in a different animal model. To further investigate how total energy plays a role in hemorrhage an experimental study was conducted.

4.1 Experimental settings

Data from the preliminary study indicated that total energy of 12J had the highest percentage occurrence (40%) among rat and mice. To obtain high rate of hemorrhage occurrence the settings for the experiment were based on the highest value of total energy. The exposure duration was limited to less than 4 minutes in order to simulate practical conditions of exposure. Volume of the focal region was estimated using the formula

$$\text{Volume} = \frac{\pi}{4} \left(\frac{1.02 c F \#}{f} \right)^2 \left(\frac{7.01 c (F \#)^2}{f} \right) \tag{4.1}$$

where c is the speed of sound in the medium; F# is focal number and is given by the ratio of the focal length to the diameter of the aperture; f is the frequency of the wave. A high pulse repetition frequency was selected so that more ultrasound pulses could hit the boundary thus helping to evaluate the effect of mechanical force on the tissue. Numbers of pulses were

calculated by taking the product of pulse repetition frequency and exposure duration. Energy density of the wave was calculated by dividing the total energy by the product of number of pulses and volume of the focal region. Energy density was multiplied by the speed of sound in water (1540 m/s) to give the pulse average intensity of the wave. KZK (Khokhlov-Zabolotskaya-Kuznetsov) equations were solved to find the values of peak to peak voltage, rarefactional and compressional pressure corresponding to the given pulse average intensity. A case was taken in which the total energy was increased to 15J to see if the trend had any threshold limit for rarefactional pressure or was only dependent on the total energy. The exposure conditions are not in the diagnostic level but are approaching.

4.2 Experimental Protocol

The major challenge faced by previous investigators was to align the ultrasound beam with the fetal head. Dalecki et al. took the approach of aligning the beam through the mother's skin, resulting in exposures all over the fetal body. To focus the ultrasound beam more precisely, Bigelow et al. made an incision in the pelvic region to pull the tissue layers back revealing the uterus containing the developing fetuses. The method proved more effective but exposures were still found on sham groups as the fetus could still move inside the uterus. To provide a more effective way the possibility of controlling the fetal movement was studied. The best way to implement it was a different animal model and a separate positioning system for the fetus, to perfectly align the ultrasound beam.

The Brazilian opossums (Monodelphis domestica) are considered an emerging animal model system for basic research into the development and regeneration of the mammalian nervous system. Developmental studies are carried out on a regular basis requiring new born opossum pups. The young are born in an extremely immature state after a 14-day gestation (typically 19-21 day gestation for mice and rats) and the pups undergo a protracted period of postnatal development. Because they are pouchless marsupials, the lack of pouch facilitates early experimental and/or surgical manipulations and therefore circumvents in utero surgical procedures that would be required on mice or rats.

Institutional Animal Care and Use Committee at Iowa State University approved the animal protocol and were in accordance with all the National Institute of Health (NIH) rules for the human use of laboratory animals. 7-8 days old post natal opossum pups were anesthetized with 65-87 mg/kg sodium pentobarbital administered subcutaneously in the caudal half of the body. The pups were detached one by one from the mother so that stress on the mother and pup could be avoided. The pups were rested on a warm bed while waiting to become unconscious.

Pups were deeply anesthetized about 5 minutes after administration of anesthesia. Anesthetized pups were gently attached to a rod using electrical tape, the rod was inverted, and the frontal and parietal areas of the skulls were positioned in a tank containing degassed distilled water at 37°C. The rod was then attached to a three Axis computer controlled positioning system (BiSlide Assemblies, VELMEX Inc., Bloomfield, NY). A 1.1 MHz spherically focused transducer (H-101, Sonic Concepts, Inc., Bothell, MA) of focal length 6.34 cm and an active diameter of 6.36 cm was hooked to a second VELMEX

positioning system. After focusing the transducer at the water surface; the animal was lowered onto the water surface. A pulser/receiver (Parametrics 5900 PR, Waltham, MA) was excited to locate the fetal skull, which could be seen by disappearing of echo lines. The pup was moved until the transducer was perfectly aligned with the back of the fetal skull. A high power amplifier (55 dB gain, 1140LA-CI, Electronics & Innovation Ltd., Rochester, NY) was used for the HIFU exposure. Figure 5 shows the setup.

Table 2. Overview of exposure parameters

Exposure	P_c, P_R(MPa)	PRF(Hz)	I_{TA}(mW/cm^2)	E.D (Sec)	Total Energy(J)
Sham	1.1, 1.1	500	0	240	0
A	10.45,6.0	500	8.92	180	12
B	6.42,4.5	500	4.46	240	12
C	5.1,3.62	1000	5.57	240	15

A sine pulse of 1.1 MHz with 10 cycles and a pulse duration of 1.1 µs was used to expose three different groups A, B, C (n=8) and one control group (n=8) in random order. Table 2 shows the exposure conditions used for the four groups. All the settings were varied by varying the PRF and the exposure duration. Group A and Group B had the same total energy but different exposure durations, hence different I_{TA}. The aim was to see how higher I_{TA} and higher rarefactional pressure affect the occurrence rate and area of damage. Group C had higher total energy than groups A and B, but has the same exposure duration as group B. The PRF for group C was doubled to increase the number of pulses, even at lower values of I_{TA} and rarefractional pressure, and observe if the hemorrhage area and occurrence are still

predominated by the total energy term. Groups A, B, C along with the control group were examined for hemorrhage. The area of hemorrhage was measured using vernier calipers after exposure. The damaged area was estimated as an ellipse and the major and minor axis were measured for an estimate of area. The pups were humanely euthanized with an intra-peritoneal overdose of sodium pentobarbital.

CHAPTER 5. RESULTS & DISCUSSION

The data obtained from experimental study on opossum pups was put together with the previous data from rats and mice to see if the trend continued. All the dependencies were plotted again to study the correlation with hemorrhage area and occurrence.

5.1 Results

Hemorrhage area and occurrence were plotted against I_{SPTA}, p_r, p_r/f, $(p_r*PRF)/f$, ED, N, ED*N, TE, $I_{PA}*$ beam area*N. Figure 6(a) shows the percentage occurrence of hemorrhage and summarizes it in table 3. Exposure A has highest percentage of occurrence. Exposure C has higher total energy compared to exposure A but has lower occurrence rate. Figure 6(b) shows the area of hemorrhage for different exposure conditions; again group A has the highest area, Group C has the highest total energy but lowest area.

Table 3. Hemorrhage area and occurrence

Exposure	% occurrence	Area
Sham	0	0
A	37.5	4.596±0.159
B	25	3.695±0.162
C	25	3.514±0.082
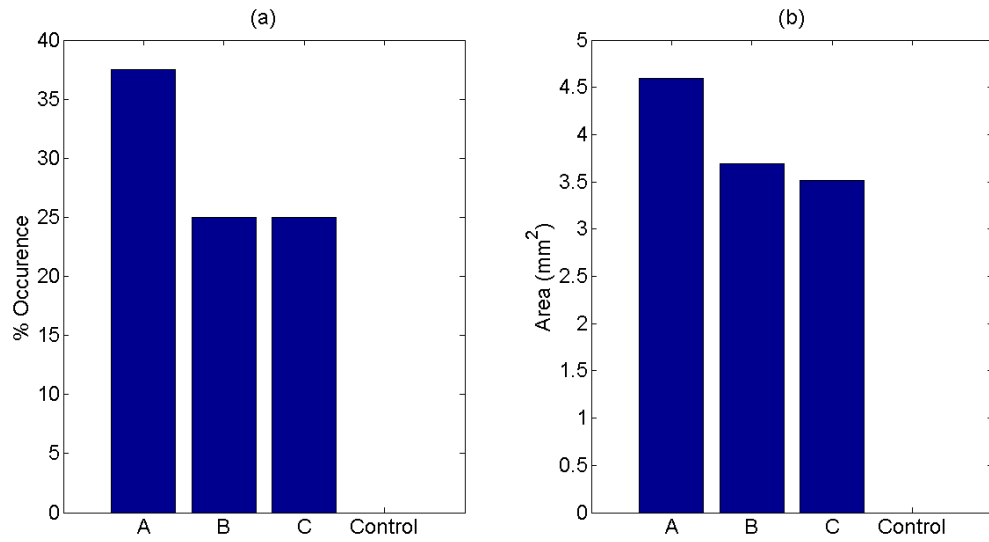
Figure 6. Hemorrhage occurrence and area for opossum fetus

Figure 7. Correlation of hemorrhage occurrence with different exposure parameters including (a) spatial peak temporal average intensity, (b) rarefactional pressure, (c) rarefactional pressure per frequency, (d) product of rarefactional pressure per frequency and pulse repletion frequency

Figure 8. Correlation of hemorrhage occurrence with different exposure parameters including (a) energy density, (b) number of pulses, (c) product of energy density and number of pulses, (d) total energy
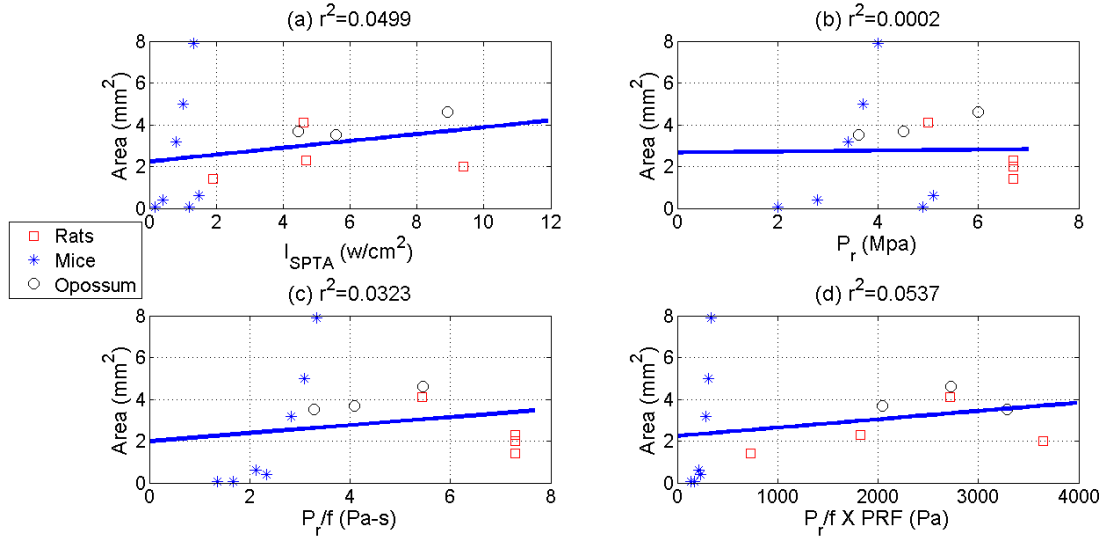
Figure 9. Correlation of hemorrhage area with different exposure parameters including (a) spatial peak temporal average intensity, (b) rarefactional pressure, (c) rarefactional pressure per frequency, (d) product of rarefactional pressure per frequency and pulse repletion frequency

Figure 7, figure 8 shows the percentage occurrence plotted against different parameters. The r^2 values are similar to those observed in mice and rats with total energy having the highest correlation with hemorrhage occurrence. Figure 9 and figure 10 depict the area of hemorrhage against all parameters along with their r^2 values. Figure 11 finds the correlation between hemorrhage occurrences and area with the surface power term.
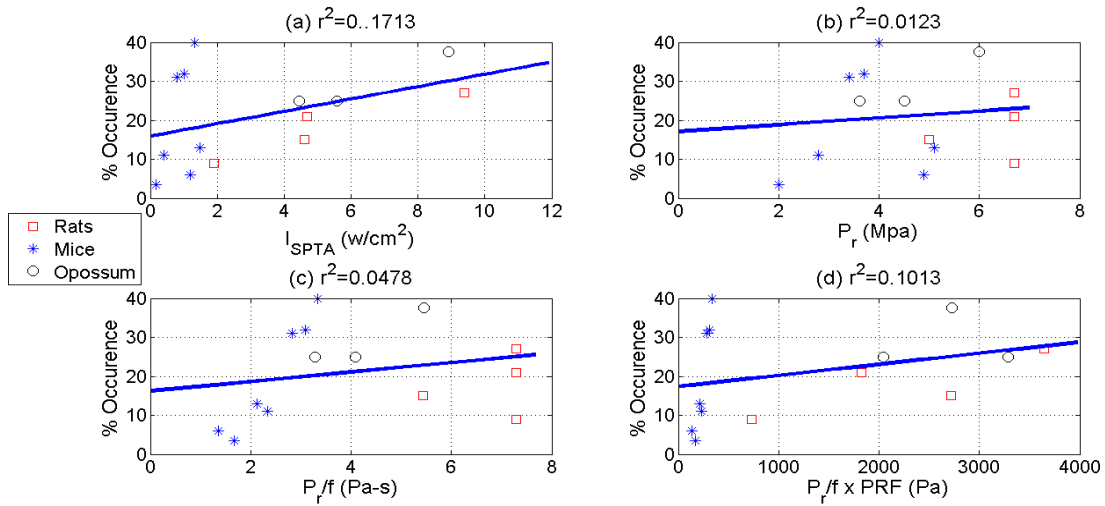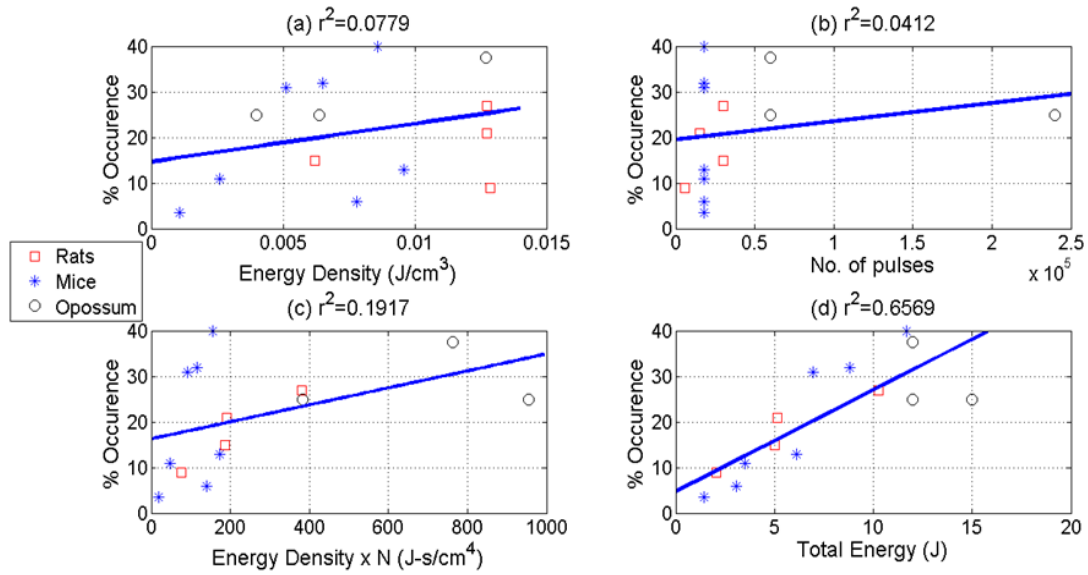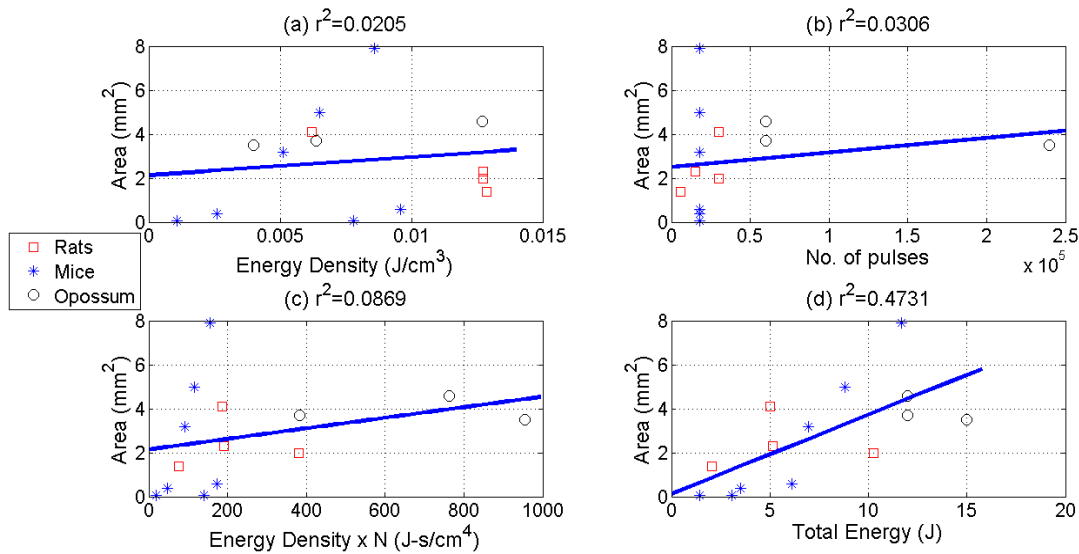

Figure 10. Correlation of hemorrhage area with different exposure parameters including (a) energy density, (b) number of pulses, (c) product of energy density and number of pulses, (d) total energy

The I_{TA} does not show a good linear trend against occurrence and area indicating that the hemorrhage is not due to thermal heating. Lack of dependence on peak rarefactional pressure, peak rarefactional pressure divided by frequency and product of peak rarefactional pressure divided by frequency and pulse repetition frequency suggests that inertial cavitation is unlikely. Furthermore there is an absence of nuclei for cavitation. Energy density and

number of pulses also do not show any correlation with occurrence and hemorrhage. Product of energy density and number of pulses shows a good linear trend if only rat and opossum are
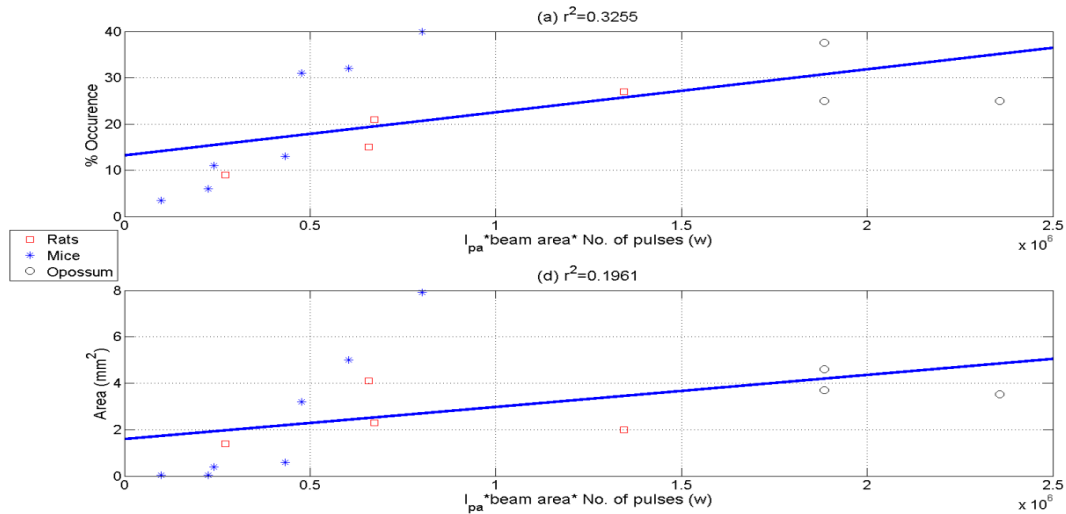
Figure 11. Correlation of product of pulse average intensity, beam area and number of pulses with (a) hemorrhage occurrence, (b) hemorrhage area

considered. The total energy term show a strong linear dependence on percentage occurrence and hemorrhage. No percentage occurrence and hemorrhage area was found for control group. The use of two positioning system ensured a very high success in alignment process which was observed with 100% hemorrhage when opossum pups were exposed to higher rarefactional values. Hemorrhage was observed closed to eyes, back of head and near suture lines.

5.2 Discussion

Hemorrhage occurrence and area correlates with total energy term, which is made up of energy density, number of pulse and volume of the focal region. Energy density term indicates that the hemorrhage is due to the force exerted by the ultrasound pulse which suggests radiation force or mechanical damage as the possible mechanism, although there is no direct dependence on energy density. The number of pulses increases the repetitive damage done to the tissue whereas the volume of the focal region considers the possibility of hitting a weak spot in the region. The damage might be mechanical in nature which may be caused by the repetitive hitting of ultrasonic pulses on the skull. The low occurrence and area for group C, which has higher total energy, suggests that a pressure or intensity may be more important than originally thought for. The hemorrhage is hypothesized to occur because of ultrasonic wave pushing the ostracizing skull into blood vessels thereby puncturing them and causing hemorrhage, the volume term considers the probability of having such a weak area in the exposure location. To prove that the hypothesis stands valid, an experiment to determine the mechanical properties of opossum pups is required. Although diagnostic ultrasound operates at lower rarefactional pressure values, the exposure duration should be kept at minimum because total energy increases with exposure duration. We hypothesize that the hemorrhage might be due to repetitive hitting of ultrasound beam on the soft ossifying bone. The ruptured soft bone may press into surrounding blood vessels and cause the hemorrhage. The slight dependence on the surface power suggests that hemorrhage might occur due to radiation pressure or mechanical fatigue.

Since the hemorrhage area from exposure A is statistically different from exposure B and exposure C with p values of 0.0086 and 0.0033 respectively, there should be a dependence on the surface term. The poor correlation with surface term guided us to reevaluate the surface power term. As the force applied on the skull is increased, the number of cycles for fatigue damage should decrease, but this decrease is not linear in nature. To model this non linearity the number of pulses was decided to vary with power law rather than a linear variation. The modified total energy and surface power can now be expressed as

$$TE = Energy\ density * volume\ of\ focal\ region * (number\ of\ pulses)^b \qquad (5.1)$$

$$SP = Pulse\ average\ intensity * beam\ area * (number\ of\ pulses)^b \qquad (5.2)$$

where b is a real number.

To optimize the total energy and surface power term the value of b was varied from 0 to 1. The highest r^2 value would correspond to the best fit. Table 4 shows the highest r^2 values for different total energy and surface power term.

Table 4. Best fit values for b

Dependency	Hemorrhage	r^2 value	b
Total Energy	Occurrence	0.8872	0.74
Total Energy	Area	0.6686	0.72
Surface power	Occurrence	0.6408	0.51
Surface power	Area	0.3930	0.48

Average b value of 0.73 was chosen for the modified total energy term whereas average b value of 0.50 was chosen for surface power term. Figure 12(a) and figure 12(b) show the modified total energy versus hemorrhage occurrence and area. Figure 13(a) and

figure 13(b) show the modified surface power plotted against hemorrhage occurrence and area.
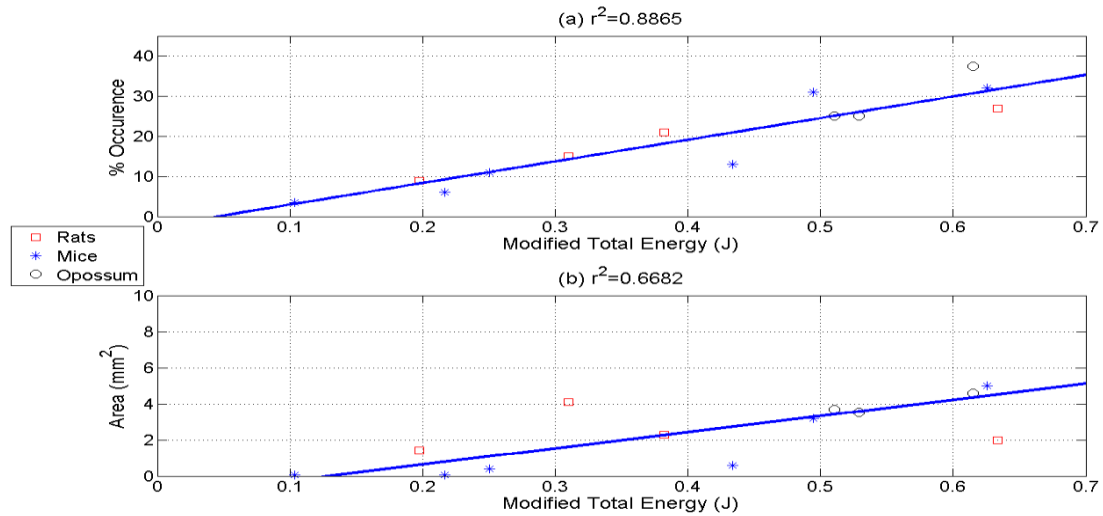
Figure 12. Correlation of modified total energy (product of energy density, volume of the focal region and number of pulses raised to 0.73) with (a) hemorrhage occurrence, (b) hemorrhage area
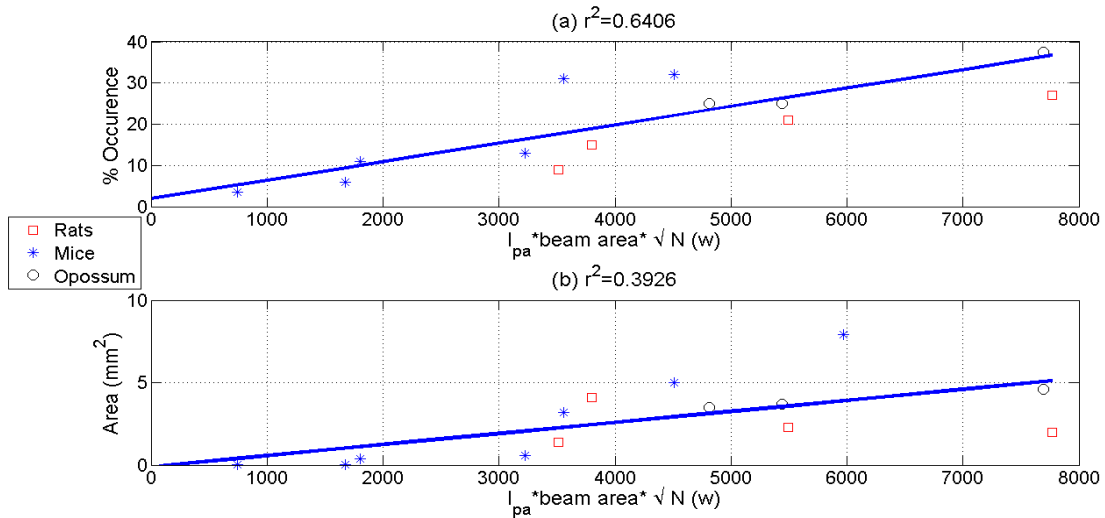
Figure 13. Correlation of modified surface power (product of pulse average intensity, beam area and square root of number of pulses) with (a) hemorrhage occurrence, (b) hemorrhage area

5.3 Application at diagnostic levels

To study the effects of modified total energy and modified surface power term at diagnostic levels, a small study was conducted. The following parameters were taken for the study. The FDA approved limit for temporal average intensity for diagnostic purposes is $720mW/cm^2$. Based on this limit, safe exposure duration can be calculated for 20% hemorrhage. An obstetrics transducer operates at a frequency of 2.5MHz - 3.5MHz.
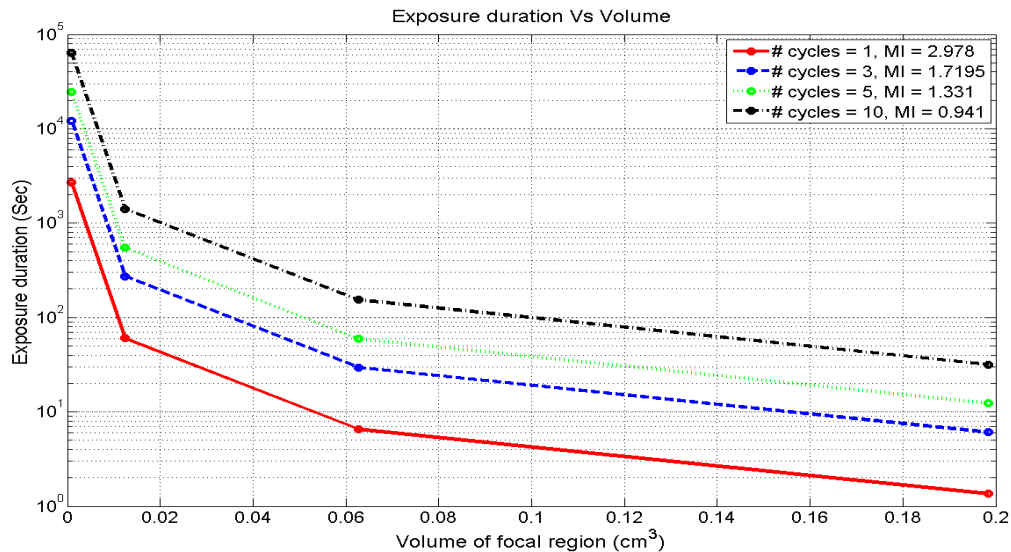
Figure 14. Plot of exposure duration vs. volume with varying number of cycles

Modified total energy for 20% hemorrhage is nearly 0.42 Joules from figure 8. The average PRF used for diagnostic purposes is 2.5 KHz. Since F# changes from transducer to transducer, F#1, 2, 3, 4 is considered. Number of cycles is varied from 1, 3, 5, and 10 to cover all possible cases. Currently the FDA stipulates a maximum limit for mechanical index that diagnostic ultrasound scanners cannot exceed as 1.9. Mechanical index can be used as an

estimate for the degree of bio-effects a given set of ultrasound parameters will induce. A higher mechanical index means a larger risk for a bio-effect. Mechanical index can be calculated by the ratio of peak negative pressure to the square root of the central frequency. Figure 14 shows the exposure duration versus volume of focal region with varying number of cycles along with the mechanical index induced by them. The circles in the plot correspond to the varying F# of 1 to 4 from left to right. From the graph we can say that if we are targeting a tissue region with an approximate volume of 0.04 cm^3, with 3 cycles, there is a 20% chance of causing hemorrhage within the first 80 seconds.
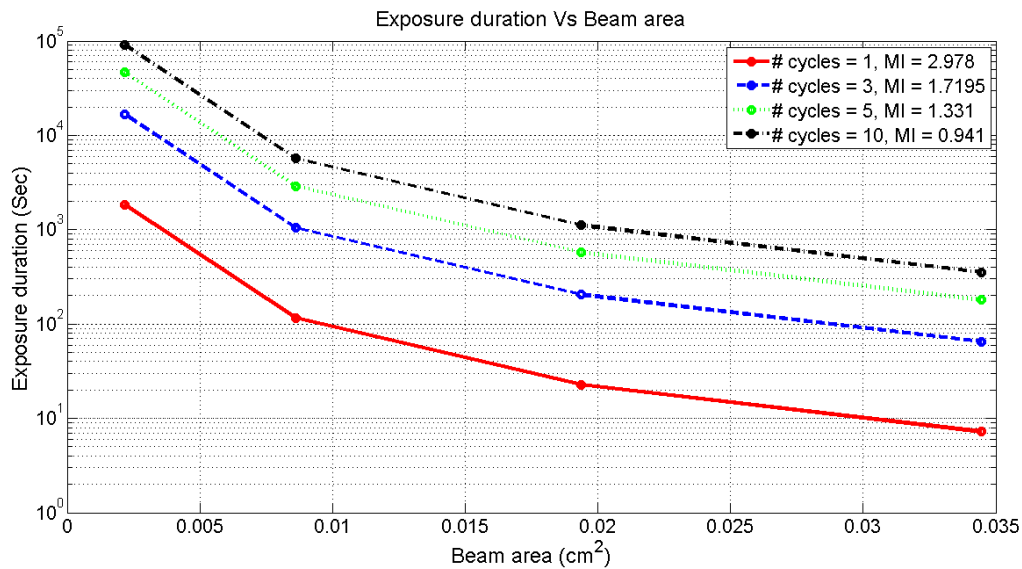
Figure 15. Plot of exposure duration vs. beam area with varying number of cycles

A similar graph was plotted for the surface power term using the same value for temporal average intensity, frequency, pulse repetition frequency, F#, number of cycles, mechanical index. The modified surface power corresponding to 20% hemorrhage occurrence is 4000 Watts. Figure 15 plots the exposure duration against beam area with

varying number of cycles along with the mechanical index induced by them. From the graph we can say that if we are targeting a tissue region with an approximate area of 0.015 cm^2, with 3 cycles, there is a 20% chance of causing hemorrhage within the first 400 seconds. With the help of figure 14 and figure 15, the safe limit for exposure time for a given volume or area can be determined.

The study identifies the ultrasound parameter related with hemorrhage although the mechanism behind the hemorrhage still needs to be studied. More research is required in this field before the application of ultrasound in noninvasive therapeutic applications.

APPENDIX

Table A. Defects that have benefited from fetal surgery

Defect	Effect on Development	Results without Treatment
Urinary Tract Obstruction	Hydronephrosis	Renal Failure
	Lung Hypoplasia	Respiratory Insufficiency
Congenital Diaphragmatic Hernia (Hole in diaphragm)	Lung Hypoplasia	Respiratory Insufficiency Pulmonary Hypertension
Cystic Adenomatoid Malformation	Lung Hypoplasia	Respiratory Insufficiency Fetal Hydrops
Sacrococcygeal Teratoma	High-Output Heart Failure	Fetal Hydrops, Fetal Demise
Placental Vascular Anomalies	Vascular "Steal" Through Placenta	Fetal Hydrops, Fetal Demise
Aqueductal Stenosis	Fluid in Brain	Brain Damage
Complete Heart Block	Low-Output Heart Failure	Fetal Hydrops, Fetal Demise
Pulmonary-Aortic Obstruction	Ventricular Hypertrophy	Heart Failure
Congenital High Airway Obstruction Syndrome	Overdistension by Lung Fluid	Fetal Hydrops Fetal Demise
Spina Bifida	Spinal Cord Damage Fluid in Brain Chiari Malformation	Paralysis Neurogenic Bladder Orthopedic Anomalies
Fetal Hydrothorax	Lung Hypoplasia	Respiratory Failure
Amniotic Band Syndrome	Limb/Digit Amputation Umbilical Cord Constriction	Persistent Deformity Fetal Demise
Cleft Lip and Palate	Facial Defect	Persistent Deformity
Twin-Twin Transfusion Syndrome	Blood Flow Imbalance	Fetal Demise Neurodevelopmental Anomalies
Twin Reversed Arterial Perfusion Syndrome	High-Output Heart Failure	Fetal Demise

REFERENCES

[1]   E. Danzer, R. M. Sydorak, M. R. Harrison, and C. T. Albanese, "Minimal access fetal surgery," *European Journal of Obstetrics & Gynecology and Reproductive Biology,* vol. 108, pp. 3-13, 2003.

[2]   J. L. Foley, J. W. Little, F. L. Starr III, C. Frantz, and S. Vaezy, "Image-guided HIFU neurolysis of peripheral nerves to treat spasticity and pain," *Ultrasound in Medicine & Biology,* vol. 30, pp. 1199-1207, 2004.

[3]   K. Hynynen, "Review of ultrasound therapy," in *IEEE Ultrasonics Symposium*, 1997, pp. 1305-1313.

[4]   F. L. Lizzi, J. Driller, B. Lunzer, A. Kalisz, and D. J. Coleman, "Computer model of ultrasonic hyperthermia and ablation for ocular tumors using b-mode data," *Ultrasound in Medicine & Biology,* vol. 18, pp. 59-73, 1992.

[5]   R. Otsuka, K. Fujikura, K. Hirata, T. Pulerwitz, Y. Oe, T. Suzuki, R. Sciacca, C. Marboe, J. Wang, D. Burkhoff, R. Muratore, F. L. Lizzi, and S. Homma, "In vitro ablation of cardiac valves using high-intensity focused ultrasound," *Ultrasound in Medicine & Biology,* vol. 31, pp. 109-114, 2005.

[6]   R. Souchon, O. Rouviere, A. Gelet, V. Detti, S. Srinivasan, J. Ophir, and J.-Y. Chapelon, "Visualisation of HIFU lesions using elastography of the human prostate in vivo: preliminary results," *Ultrasound in Medicine & Biology,* vol. 29, pp. 1007-1015, 2003.

[7]   K. Takegami, Y. Kaneko, T. Watanabe, T. Maruyama, Y. Matsumoto, and H. Nagawa, "Erythrocytes, as well as microbubble contrast agents, are important factors in improving thermal and therapeutic effects of high-intensity focused ultrasound," *Ultrasound in Medicine & Biology,* vol. 31, pp. 385-390, 2005.

[8]   F. Wu, Z.-B. Wang, P. Lu, Z.-L. Xu, W.-Z. Chen, H. Zhu, and C.-B. Jin, "Activated anti-tumor immunity in cancer patients after high intensity focused ultrasound ablation," *Ultrasound in Medicine & Biology,* vol. 30, pp. 1217-1222, 2004.

[9]   J. E. Parsons, C. A. Cain, G. D. Abrams, and J. B. Fowlkes, "Pulsed cavitational ultrasound therapy for controlled tissue homogenization," *Ultrasound in Medicine & Biology,* vol. 32, pp. 115-129, 2006.

[10]   Z. Xu, J. B. Fowlkes, E. D. Rothman, A. M. Levin, and C. A. Cain, "Controlled ultrasound tissue erosion: The role of dynamic interaction between insonation and microbubble activity," *The Journal of the Acoustical Society of America,* vol. 117, pp. 424-435, 2005.

[11]   Z. Xu, A. Ludomirsky, L. Y. Eun, T. L. Hall, B. C. Tran, J. B. Fowlkes, and C. A. Cain, "Controlled ultrasound tissue erosion," *Ultrasonics, Ferroelectrics and Frequency Control, IEEE Transactions on,* vol. 51, pp. 726-736, 2004.

[12]   M. Duvshani-Eshet and M. Machluf, "Therapeutic ultrasound optimization for gene delivery: A key factor achieving nuclear DNA localization," *Journal of Controlled Release,* vol. 108, pp. 513-528, 2005.

[13]   J. L. B. Feril, R. Ogawa, H. Kobayashi, H. Kikuchi, and T. Kondo, "Ultrasound enhances liposome-mediated gene transfection," *Ultrasonics Sonochemistry,* vol. 12, pp. 489-493, 2005.

[14]   J. P. Christiansen, B. A. French, A. L. Klibanov, S. Kaul, and J. R. Lindner, "Targeted tissue transfection with ultrasound destruction of plasmid-bearing cationic microbubbles," *Ultrasound in Medicine & Biology,* vol. 29, pp. 1759-1767, 2003.

[15] P. A. Frenkel, S. Chen, T. Thai, R. V. Shohet, and P. A. Grayburn, "Dna-loaded albumin microbubbles enhance ultrasound-mediated transfection in vitro," *Ultrasound in Medicine & Biology,* vol. 28, pp. 817-822, 2002.

[16] H.-D. Liang, Q. L. Lu, S.-A. Xue, M. Halliwell, T. Kodama, D. O. Cosgrove, H. J. Stauss, T. A. Partridge, and M. J. K. Blomley, "Optimisation of ultrasound-mediated gene transfer (sonoporation) in skeletal muscle cells," *Ultrasound in Medicine & Biology,* vol. 30, pp. 1523-1529, 2004.

[17] Y. Manome, N. Nakayama, K. Nakayama, and H. Furuhata, "Insonation facilitates plasmid DNA transfection into the central nervous system and microbubbles enhance the effect," *Ultrasound in Medicine & Biology,* vol. 31, pp. 693-702, 2005.

[18] R. Ogawa, T. Kondo, H. Honda, Q. L. Zhao, S. Fukuda, and P. Riesz, "Effects of dissolved gases and an echo contrast agent on ultrasound mediated in vitro gene transfection," *Ultrasonics Sonochemistry,* vol. 9, pp. 197-203, 2002.

[19] W. Wei, B. Zhengzhong, W. Yongjie, Y. Lafeng, and M. Yalin, "A novel approach to quantitative ultrasonic naked gene delivery and its non-invasive assessment," *Ultrasonics,* vol. 43, pp. 69-77, 2004.

[20] V. G. Zarnitsyn and M. R. Prausnitz, "Physical parameters influencing optimization of ultrasound-mediated DNA transfection," *Ultrasound in Medicine & Biology,* vol. 30, pp. 527-538, 2004.

[21] M. J. Shortencarier, P. A. Dayton, S. H. Bloch, P. A. Schumann, T. O. Matsunaga, and K. W. Ferrara, "A method for radiation-force localized drug delivery using gas-filled lipospheres," *Ultrasonics, Ferroelectrics and Frequency Control, IEEE Transactions on,* vol. 51, pp. 822-831, 2004.

[22] A. van Wamel, A. Bouakaz, B. Bernard, F. ten Cate, and N. de Jong, "Radionuclide tumour therapy with ultrasound contrast microbubbles," *Ultrasonics,* vol. 42, pp. 903-906, 2004.

[23] E. C. Everbach and C. W. Francis, "Cavitational mechanisms in ultrasound-accelerated thrombolysis at 1 MHz," *Ultrasound in Medicine & Biology,* vol. 26, pp. 1153-1160, 2000.

[24] H. W. Fulghum and E. P. Vasquez, "Congenital cystic adenomatoid malformation: A case study," *The Internet Journal of Advanced Nursing Practice,* vol. 5, pp. 1-7, 2003.

[25] H. L. Hedrick, A. W. Flake, T. M. Crombleholme, L. J. Howell, M. P. Johnson, R. D. Wilson, and N. S. Adzick, "Sacrococcygeal teratoma: prenatal assessment, fetal intervention, and outcome," *Journal of Pediatric Surgery,* vol. 39, pp. 430-438, 2004.

[26] C. Fox, M. D. Kilby, and K. S. Khan, "Contemporary treatments for twin-twin transfusion syndrome," *Obstet Gynecol,* vol. 105, pp. 1469-1477, June 1, 2005 2005.

[27] K. Sasaki, S.-i. Umemura, K. Ichizuka, T. Okai, M. Ichihara, S. Ando, and M. Kushima, "Fetal vascular occlusion by using high-intensity focused ultrasound; To investigate the potential for the treatment of twin reversed arterial perfusion syndrome," in *5th International Symposium on Therapeutic Ultrasound*, Boston, MA, 2005.

[28] S. B. Barnett, G. R. Ter Haar, M. C. Ziskin, W. L. Nyborg, K. Maeda, and J. Bang, "Current status of research on biophysical effects of ultrasound," *Ultrasound in Medicine & Biology,* vol. 20, pp. 205-218, 1994.

[29] T. A. Bigelow and W. D. O'Brien, Jr., "Estimating the Thermal Dose From Backscattered RF Echoes," in *4th International Symposium on Therapeutic Ultrasound*, Kyoto, Japan, 2005, pp. 151-153.

[30] W. D. O'Brien, Jr. and T. A. Siddiqi, "Obstetric Sonography: The output display standard and ultrasound bioeffects," in *Sonography in Obstetrics and Gynecology: Principles and Practice*,

A. C. Fleischer, F. A. Manning, P. Jeanty, and R. Romero, Eds., 6th ed NY: McGraw-Hill, 2001, pp. 29-48.

[31]   J. G. Abbott, "Rationale and derivation of MI and TI--a review," *Ultrasound in Medicine & Biology,* vol. 25, pp. 431-441, 1999.

[32]   E. L. Carstensen, S. Z. Child, S. Norton, and W. Nyborg, "Ultrasonic heating of the skull," *The Journal of the Acoustical Society of America,* vol. 87, pp. 1310-1317, 1990.

[33]   C. Doody, F. A. Duck, and V. F. Humphrey, "Comparison of finite element and heated disc models of tissue heating by ultrasound," *Ultrasound in Medicine & Biology,* vol. 26, pp. 1347-1355, 2000.

[34]   J. L. Drewniak, K. I. Carnes, and F. Dunn, "In vitro ultrasonic heating of fetal bone," *The Journal of the Acoustical Society of America,* vol. 86, pp. 1254-1258, 1989.

[35]   B. A. Herman and M. R. Myers, "An analytic derivation for the transient temperature rise during an ultrasound pulse focused on bone," *Ultrasound in Medicine & Biology,* vol. 29, pp. 771-773, 2003.

[36]   J. R. Jago, J. Henderson, T. A. Whittingham, and G. Mitchell, "A comparison of AIUM/NEMA thermal indices with calculated temperature rises for a simple third-trimester pregnancy tissue model," *Ultrasound in Medicine & Biology,* vol. 25, pp. 623-628, 1999.

[37]   M. R. Myers, "Effect of pulse characteristics on temperature rise due to ultrasound absorption at a bone/soft-tissue interface," *The Journal of the Acoustical Society of America,* vol. 117, pp. 3281-3287, 2005.

[38]   T. P. O'Neill, A. J. Winkler, and J. Wu, "Ultrasound heating in a tissue-bone phantom," *Ultrasound in Medicine & Biology,* vol. 20, pp. 579-588, 1994.

[39]   J. Wu and G. Du, "Temperature elevation generated by a focused Gaussian ultrasonic beam at a tissue--bone interface," *The Journal of the Acoustical Society of America,* vol. 87, pp. 2748-2755, 1990.

[40]   J. S. Abramowicz, S. B. Barnett, F. A. Duck, P. D. Edmonds, K. H. Hynynen, and M. C. Ziskin, "Fetal thermal effects of diagnostic ultrasound," *J Ultrasound Med,* vol. 27, pp. 541-59; quiz 560-3, Apr 2008.

[41]   W. L. Nyborg, "Solutions of the bio-heat transfer equation," *Physics in Medicine and Biology,* vol. 33, p. 785, 1988.

[42]   S. B. Barnett, "Intracranial temperature elevation from diagnostic ultrasound," *Ultrasound in Medicine & Biology,* vol. 27, pp. 883-888, 2001.

[43]   P. M. Duggan, G. C. Liggins, and S. B. Barnett, "Ultrasonic heating of the brain of the fetal sheep in utero," *Ultrasound in Medicine & Biology,* vol. 21, pp. 553-560, 1995.

[44]   M. M. Horder, S. B. Barnett, G. J. Vella, and M. J. Edwards, "Ultrasound-induced temperature increase in the guinea-pig fetal brain in vitro," *Ultrasound in Medicine & Biology,* vol. 24, pp. 697-704, 1998.

[45]   M. M. Horder, S. B. Barnett, G. J. Vella, and M. J. Edwards, "Effects of pulsed ultrasound on sphenoid bone temperature and the heart rate in guinea-pig foetuses," *Early Human Development,* vol. 52, pp. 221-233, 1998.

[46]   M. M. Horder, S. B. Barnett, G. J. Vella, M. J. Edwards, and A. K. W. Wood, "In vivo heating of the guinea-pig fetal brain by pulsed ultrasound and estimates of thermal index," *Ultrasound in Medicine & Biology,* vol. 24, pp. 1467-1474, 1998.

[47]   M. M. Horder, S. B. Barnett, G. J. Vella, M. J. Edwards, and A. K. W. Wood, "Ultrasound-induced temperature increase in guinea-pig fetal brain in utero: third-trimester gestation," *Ultrasound in Medicine & Biology,* vol. 24, pp. 1501-1510, 1998.

[48]   P. R. Stone, I. Ross, K. Pringle, and J. Flower, "Tissue heating effect of pulsed Doppler ultrasound in the live fetal lamb brain," *Fetal Diagn Ther,* vol. 7, pp. 26-30, 1992 1992.

[49]   F. Jenson, F. Padilla, V. Bousson, C. Bergot, J. D. Laredo, and P. Laugier, "In vitro ultrasonic characterization of human cancellous femoral bone using transmission and backscatter measurements: Relationships to bone mineral density," *The Journal of the Acoustical Society of America,* vol. 119, pp. 654-663, 2006.

[50]   K. I. Lee, H.-S. Roh, and S. W. Yoon, "Correlations between acoustic properties and bone density in bovine cancellous bone from 0.5 to 2 MHz," *The Journal of the Acoustical Society of America,* vol. 113, pp. 2933-2938, 2003.

[51]   M. B. Tavakoli and J. A. Evans, "Dependence of the velocity and attenuation of ultrasound in bone on the mineral content," *Physics in Medicine and Biology,* vol. 36, p. 1529, 1991.

[52]   K. A. Wear, "Ultrasonic attenuation in human calcaneus from 0.2 to 1.7 MHz," *Ultrasonics, Ferroelectrics and Frequency Control, IEEE Transactions on,* vol. 48, pp. 602-608, 2001.

[53]   S. B. Barnett, "Biophysical aspects of diagnostic ultrasound," *Ultrasound in Medicine & Biology,* vol. 26, pp. S68-S70, 2000.

[54]   S. B. Barnett, H.-D. Rott, G. R. ter Haar, M. C. Ziskin, and K. Maeda, "The sensitivity of biological tissue to ultrasound," *Ultrasound in Medicine & Biology,* vol. 23, pp. 805-812, 1997.

[55]   M. J. Edwards, K. Shiota, M. S. R. Smith, and D. A. Walsh, "Hyperthermia and birth defects," *Reproductive Toxicology,* vol. 9, pp. 411-425, 1995.

[56]   AIUM, "Bioeffects and Safety of Diagnositc Ultrasound," ed. Laurel, MD: American Institute of Ultrasound in Medicine, Laurel, MD, 1993.

[57]   M. Fujii, K. Sakamoto, Y. Toda, A. Negishi, and H. Kanai, "Study of the cause of the temperature rise at the muscle-bone interface during ultrasound hyperthermia," *Biomedical Engineering, IEEE Transactions on,* vol. 46, pp. 494-504, 1999.

[58]   B. A. Haken, L. A. Frizzell, and E. L. Carstensen, "Effect of mode conversion on ultrasonic heating at tissue interfaces," *J Ultrasound Med,* vol. 11, pp. 393-405, August 1, 1992 1992.

[59]   G. J. Vella, V. F. Humphrey, F. A. Duck, and S. B. Barnett, "The cooling effect of liquid flow on the focussed ultrasound-induced heating in a simulated foetal brain," *Ultrasound in Medicine & Biology,* vol. 29, pp. 1193-1204, 2003.

[60]   G. J. Vella, V. F. Humphrey, F. A. Duck, and S. B. Barnett, "Ultrasound-induced heating in a foetal skull bone phantom and its dependence on beam width and perfusion," *Ultrasound in Medicine & Biology,* vol. 29, pp. 779-788, 2003.

[61]   C. C. Church, E. L. Carstensen, W. L. Nyborg, P. L. Carson, L. A. Frizzell, and M. R. Bailey, "The risk of exposure to diagnostic ultrasound in postnatal subjects: nonthermal mechanisms," *J Ultrasound Med,* vol. 27, pp. 565-92; quiz 593-6, Apr 2008.

[62]   H. G. Flynn, "Generation of transient cavities in liquids by microsecond pulses of ultrasound," *The Journal of the Acoustical Society of America,* vol. 72, pp. 1926-1932, 1982.

[63]   J. Wu and G. Du, "Streaming generated by a bubble in an ultrasound field," *The Journal of the Acoustical Society of America,* vol. 101, pp. 1899-1907, 1997.

[64]   R. E. Apfel and C. K. Holland, "Gauging the likelihood of cavitation from short-pulse, low-duty cycle diagnostic ultrasound," *Ultrasound in Medicine & Biology,* vol. 17, pp. 179-185, 1991.

[65]   C. K. Holland and R. E. Apfel, "An improved theory for the prediction of microcavitation thresholds," *Ultrasonics, Ferroelectrics and Frequency Control, IEEE Transactions on,* vol. 36, pp. 204-208, 1989.

[66] C. A. MacDonald, V. Sboros, J. Gomatam, S. D. Pye, C. M. Moran, and W. Norman McDicken, "A numerical investigation of the resonance of gas-filled microbubbles: resonance dependence on acoustic pressure amplitude," *Ultrasonics,* vol. 43, pp. 113-122, 2004.

[67] P. P. Chang, C. Wen-Shiang, P. D. Mourad, S. L. Poliachik, and L. A. Crum, "Thresholds for inertial cavitation in Albunex suspensions under pulsed ultrasound conditions," *Ultrasonics, Ferroelectrics and Frequency Control, IEEE Transactions on,* vol. 48, pp. 161-170, 2001.

[68] W. S. Chen, A. A. Brayman, T. J. Matula, and L. A. Crum, "Inertial cavitation dose and hemolysis produced in vitro with or without Optison(R)," *Ultrasound in Medicine & Biology,* vol. 29, pp. 725-737, 2003.

[69] E. C. Everbach, I. R. S. Makin, M. Azadniv, and R. S. Meltzer, "Correlation of ultrasound-induced hemolysis with cavitation detector output in vitro," *Ultrasound in Medicine & Biology,* vol. 23, pp. 619-624, 1997.

[70] S. I. Madanshetty, R. A. Roy, and R. E. Apfel, "Acoustic microcavitation: Its active and passive acoustic detection," *The Journal of the Acoustical Society of America,* vol. 90, pp. 1515-1526, 1991.

[71] J. Tu, T. J. Matula, A. A. Brayman, and L. A. Crum, "Inertial cavitation dose produced in ex vivo rabbit ear arteries with Optison [registered trademark] by 1-MHz pulsed ultrasound," *Ultrasound in Medicine and Biology,* vol. 32, pp. 281-288, 2006.

[72] O. A. Sapozhnikov, V. A. Khokhlova, M. R. Bailey, J. C. Williams Jr, J. A. McAteer, R. O. Cleveland, and L. A. Crum, "Effect of overpressure and pulse repetition frequency on cavitation in shock wave lithotripsy," *The Journal of the Acoustical Society of America,* vol. 112, pp. 1183-1195, 2002.

[73] H. R. Guzman, A. J. McNamara, D. X. Nguyen, and M. R. Prausnitz, "Bioeffects caused by changes in acoustic cavitation bubble density and cell concentration: a unified explanation based on cell-to-bubble ratio and blast radius," *Ultrasound in Medicine & Biology,* vol. 29, pp. 1211-1222, 2003.

[74] J. S. Allen, D. E. Kruse, P. A. Dayton, and K. W. Ferrara, "Effect of coupled oscillations on microbubble behavior," *The Journal of the Acoustical Society of America,* vol. 114, pp. 1678-1690, 2003.

[75] N. C. Skaropoulos, H. D. Yagridou, and D. P. Chrissoulidis, "Interactive resonant scattering by a cluster of air bubbles in water," *The Journal of the Acoustical Society of America,* vol. 113, pp. 3001-3011, 2003.

[76] E. A. Brujan, "The role of cavitation microjets in the therapeutic applications of ultrasound," *Ultrasound in Medicine & Biology,* vol. 30, pp. 381-387, 2004.

[77] S. M. Gracewski, H. Miao, and D. Dalecki, "Ultrasonic excitation of a bubble near a rigid or deformable sphere: Implications for ultrasonically induced hemolysis," *The Journal of the Acoustical Society of America,* vol. 117, pp. 1440-1447, 2005.

[78] J. R. Blake and D. C. Gibson, "Cavitation Bubbles Near Boundaries," *Annual Review of Fluid Mechanics,* vol. 19, pp. 99-123, 1987.

[79] K. Y. Chiu, F. T. Cheng, and H. C. Man, "Evolution of surface roughness of some metallic materials in cavitation erosion," *Ultrasonics,* vol. 43, pp. 713-716, 2005.

[80] A. Pearson, J. R. Blake, and S. R. Otto, "Jets in bubbles," *Journal of Engineering Mathematics,* vol. 48, pp. 391-412, 2004.

[81] S. Calle, J.-P. Remenieras, O. B. Matar, M. E. Hachemi, and F. Patat, "Temporal analysis of tissue displacement induced by a transient ultrasound radiation force," *The Journal of the Acoustical Society of America,* vol. 118, pp. 2829-2840, 2005.

[82] H. C. Starritt, F. A. Duck, and V. F. Humphrey, "Forces acting in the direction of propagation in pulsed ultrasound fields," *Physics in Medicine and Biology,* vol. 36, p. 1465, 1991.

[83] S. Girnyk, A. Barannik, E. Barannik, V. Tovstiak, A. Marusenko, and V. Volokhov, "The estimation of elasticity and viscosity of soft tissues in vitro using the data of remote acoustic palpation," *Ultrasound in Medicine & Biology,* vol. 32, pp. 211-219, 2006.

[84] K. R. Nightingale, M. L. Palmeri, R. W. Nightingale, and G. E. Trahey, "On the feasibility of remote palpation using acoustic radiation force," *The Journal of the Acoustical Society of America,* vol. 110, pp. 625-634, 2001.

[85] S. Chen, M. Fatemi, R. Kinnick, and J. F. Greenleaf, "Comparison of stress field forming methods for vibro-acoustography," *Ultrasonics, Ferroelectrics and Frequency Control, IEEE Transactions on,* vol. 51, pp. 313-321, 2004.

[86] E. E. Konofagou and K. Hynynen, "Localized harmonic motion imaging: theory, simulations and experiments," *Ultrasound in Medicine & Biology,* vol. 29, pp. 1405-1413, 2003.

[87] K. Nightingale, S. McAleavey, and G. Trahey, "Shear-wave generation using acoustic radiation force: in vivo and ex vivo results," *Ultrasound in Medicine & Biology,* vol. 29, pp. 1715-1723, 2003.

[88] M. F. Hamilton and D. T. Blackstock, *Nonlinear Acoustics*. San Diego, CA: Academic Press, 1998.

[89] G. R. Torr, "The acoustic radiation force," *American Journal of Physics,* vol. 52, pp. 402-408, 1984.

[90] R. T. Hekkenberg, K. Beissner, B. Zeqiri, R. A. Bezemer, and M. Hodnett, "Validated ultrasonic power measurements up to 20 w," *Ultrasound in Medicine & Biology,* vol. 27, pp. 427-438, 2001.

[91] P. A. Lewin, N. Barrie-Smith, M. Ide, K. Hynynen, and M. Macdonald, "Interlaboratory Acoustic Power Measurement," *J Ultrasound Med,* vol. 22, pp. 207-213, February 1, 2003 2003.

[92] G. S. K. Wong and L. Wu, "High power ultrasound standard," *The Journal of the Acoustical Society of America,* vol. 111, pp. 1791-1799, 2002.

[93] S. Chen, G. T. Silva, R. R. Kinnick, J. F. Greenleaf, and M. Fatemi, "Measurement of dynamic and static radiation force on a sphere," *Physical Review E (Statistical, Nonlinear, and Soft Matter Physics),* vol. 71, pp. 056618-4, 2005.

[94] F. G. Mitri, "Acoustic radiation force acting on elastic and viscoelastic spherical shells placed in a plane standing wave field," *Ultrasonics,* vol. 43, pp. 681-691, 2005.

[95] T. Hasegawa, K. Saka, N. Inoue, and K. Matsuzawa, "Acoustic radiation force experienced by a solid cylinder in a plane progressive sound field," *The Journal of the Acoustical Society of America,* vol. 83, pp. 1770-1775, 1988.

[96] F. G. Mitri, "Radiation force acting on an absorbing cylinder placed in an incident plane progressive acoustic field," *Journal of Sound and Vibration,* vol. 284, pp. 494-502, 2005.

[97] F. G. Mitri and S. Chen, "Theory of dynamic acoustic radiation force experienced by solid cylinders," *Physical Review E (Statistical, Nonlinear, and Soft Matter Physics),* vol. 71, pp. 016306-9, 2005.

[98] F. G. Mitri and M. Fatemi, "Dynamic acoustic radiation force acting on cylindrical shells: theory and simulations," *Ultrasonics,* vol. 43, pp. 435-445, 2005.

[99] F. G. Mitri, "Frequency dependence of the acoustic radiation force acting on absorbing cylindrical shells," *Ultrasonics,* vol. 43, pp. 271-277, 2005.

[100]   M. P. G. a. W. E. A. P. C. Paris, "A rational analytic theory of fatigue. ," *The Trend in Engineering* vol. 13, pp. 9-14, 1961.

[101]   D. Dalecki, S. Z. Child, C. H. Raeman, D. P. Penney, R. Mayer, C. Cox, and E. L. Carstensen, "Thresholds for fetal hemorrhages produced by a piezoelectric lithotripter," *Ultrasound in Medicine & Biology,* vol. 23, pp. 287-297, 1997.

[102]   D. Dalecki, S. Z. Child, C. H. Raeman, and C. Cox, "Hemorrhage in murine fetuses exposed to pulsed ultrasound," *Ultrasound in Medicine & Biology,* vol. 25, pp. 1139-1144, 1999.

[103]   T. A. Bigelow, R. J. Miller, J. P. Blue, Jr., and W. D. O'Brien, Jr., "Hemorrhage near fetal rat bone exposed to pulsed ultrasound," *Ultrasound Med Biol,* vol. 33, pp. 311-7, Feb 2007.

[104]   W.-S. Chen, A. A. Brayman, T. J. Matula, L. A. Crum, and M. W. Miller, "The pulse length-dependence of inertial cavitation dose and hemolysis," *Ultrasound in Medicine & Biology,* vol. 29, pp. 739-748, 2003.

ACKNOWLEDGEMENT

I would like thank my major advisor, Dr. Timothy Bigelow, whose continued support and encouragement has conveyed a spirit of hard work and commitment to research. Without his guidance and help, this dissertation would not have been possible.

I would also like to thank Dr. Kathleen Mullin and Dr. Dell Anna Giuseppe for their assistance with anesthesia administration to animals. I thank Dr. Donald S. Sakaguchi and Eun-Ah Ye for the help they provided in caring for animals.

Finally, I would like to give special thanks to my parents, and my brother for their encouragement, support, patience, and unending love.